Available online at www.sciencedirect.com

ScienceDirect

Transportation Research Procedia 62 (2022) 509–516

Transportation Research Procedia

www.elsevier.com/locate/procedia

24th EURO Working Group on Transportation Meeting, EWGT 2021, 8-10 September 2021, Aveiro, Portugal

Comparing different approaches for estimating tailpipe emissions in passenger cars

Paulo Fernandes[a,*], Elisabete Ferreira[a], Paulo Amorim[a], Margarida C. Coelho[a]

[a]*Department of Mechanical Engineering / Centre for Mechanical Technology and Automation (TEMA), University of Aveiro, Campus Universitário de Santiago, 3810-193 Aveiro, Portugal*

Abstract

Vehicles with Internal Combustion Engines (ICE) still represent the most prevalent form of road transport in Europe, being an important source of both greenhouse gases and air pollutants. In response to these concerns, Portable Emission Measurement Systems (PEMS) have been widely used by researchers to measure tailpipe emissions and to detect cheating of emissions regulations by manufacturers. This paper introduces four different approaches to estimate carbon dioxide (CO_2) and nitrogen oxides (NOx) emissions for these vehicles. These approaches were based on: i) speed intervals ($\leq$50 km.h^{-1}, 50-90 km.h^{-1}, $\geq$ 90 km.h^{-1}); ii) internally observable variables (IOVs); iii) vehicle specific power (VSP); and iv) driving volatility indicators. The development of IOVs models was made by testing the most significant parameters on CO_2 and NOx emission rates, which included the engine speed (RPM), manifold absolute pressure (MAP), and intake air temperate (IAT). VSP-modal approach centred on binning emission rates in 14 models that reflects deceleration, idling, cruise, and acceleration states. Driver volatility was characterized by means of vehicular jerk (i.e., first derivate of acceleration) using nine combinations of vehicular jerk types. To obtain real world emissions, data were collected from one petrol and one diesel passenger cars using an integrated PEMS. IOVs and jerk models based on the product of MAP and RPM presented similar CO_2 emission compared to measured values for both vehicles, but they resulted in higher overestimation of NOx than a VSP-modal approach. The proposed methodology can be extended to other individual ICE or alternative fuel vehicles for which it may be expensive to get emissions, engine, and dynamic data.

Keywords: Vehicle Emissions; Predictive Models; Speed, Internally Observable Variables; Vehicle Specific Power; Driving Volatility

1. Introduction and Research Objectives

Road traffic emissions contribute considerably to a wide range of air pollution problems, accounting for 39% of NOx emissions (an ozone precursor) in 2018 (EEA, 2020a). Emissions of these species have considerable deleterious effects on human health (Mannucci et al., 2015), with premature deaths having been attributed to exceedances of road transport type approval tests (Chossière et al., 2018). Despite the restrictive legislation for the new passenger cars launched in the European Union (EU), the average CO_2 per unit distance for vehicles was 122.4 g.km^{-1} in 2019 (EEA, 2020b). This remains well above the EU target of 95 g.km^{-1} for 2020. Since ICE petrol- and diesel-fuelled vehicles still represent more than 85% of total EU sales in 2019 (ACEA, 2020), there is a need for stringent NOx limits, as well

10.1016/j.trpro.2022.02.063

as to minimize tailpipe CO_2 emissions. In September of 2017, a new homologation procedure was implemented including the measurement of emissions under real driving conditions (Real Driving Emission – RDE). Since then, emission measurement studies have been conducted for petrol [e.g. (Gastaldi et al., 2017; Kurtyka and Pielecha, 2019; Davison et al., 2020)], diesel [e.g., (Davison et al., 2020; Fernandes et al., 2019; García-Contreras et al., 2020; Söderena et al., 2020; Triantafyllopoulos et al., 2019)] and hybrid [e.g. (Fernandes et al., 2021; Lijewski et al., 2020)] passenger cars to evaluate their pollutant emissions obtained under RDE driving conditions.

Owing to the high costs, time consuming to measure many vehicles and capture important variations in environmental conditions, vehicle ages and deterioration, and stricter procedure of PEMS data collection, researchers have been focused on the development of methodologies to predict exhaust emissions under RDE. Some of these include the use on-board diagnostic reader (OBD) reported data. Hu et al. (2016) developed an empirical-based approach to establish correlations between IOVs, concretely the product of manifold air pressure and revolutions per minute ($P_{MAP \times RPM}$) and emission rates in petrol passenger cars. Fernandes et al. (2019) showed that IOVs were an appropriate tool for predicting CO_2 emission rates ($R^2 > 0.8$) in four different diesel passenger cars, but they are not appropriate enough for predictions of NOx emissions ($R^2 < 0.6$) since specific parameters related to the thermal management on after treatment system were not included in their models. Another extensively used approach is the estimate of fuel use and pollutant emissions through the concept of vehicle specific power – VSP [e.g., (Coelho et al., 2009; Faria et al., 2017; Davison et al., 2020; Fernandes et al., 2021)]. Variability in second-by-second exhaust emissions in what respects to the car operation is associated with speed, acceleration, and grade (Boroujeni and Frey, 2014), which are used to compute VSP (USEPA, 2002). The interest in the driving volatility concept also has compelled researchers to predict emissions in passenger cars under RDE. Fernandes et al. (2021) presented a model, which estimated CO_2 and NOx emission rates as a function of nine classes of vehicular jerk to represent different driving behaviours. Results indicated that the developed models also yielded lower relative mean square errors than the VSP modal approach. Only one hybrid powertrain was used in the emission measurement to feed into the models, however, limiting its applicability. Since second-by-second vehicle dynamic data are often difficult to obtain for an entire fleet in a road, a common approach is to develop emissions using macroscopic models such as EPA's MOtor Vehicle Emission Simulator (MOVES) (EPA, 2020) and computer programme to calculate emissions from road transport (COPERT) (Emisia, 2020), which use average speed by trip or road type, and vehicle kilometres travelled. Macedo et al. (2020) developed a COPERT-based approximation approach to estimate CO_2 and NOx for a representative car and based on average speed intervals ($\leq$ 50 km.h^{-1}, 50-90 km.h^{-1}, $\geq$ 90 km.h^{-1}). They showed that proposed models better reflected variability on CO_2 than VSP and COPERT-based approaches.

Bearing in mind the need for a robust analysis of different approaches for predicting tailpipe emissions, this work develops second-by-second CO_2 and NOx predictive models for ICE, based on followings: i) route type, expressed in terms of speed intervals ($\leq$50 km.h^{-1}, 50-90 km.h^{-1}, $\geq$ 90 km.h^{-1}); ii) engine parameters; iii) VSP modal emission approach; iv) driving volatility as a means of vehicular jerk classification. The novelty of this paper is that i) it compares predictive emission models using externally observable variables, such as speed and VSP [(only covered approach by Macedo et al. (2020)], IOVs [(only applied method by Fernandes et al. (2019)] and driving volatility based-analysis [(Fernandes et al. (2021) only used this procedure) for different powertrains in passenger cars under RDE conditions; ii) the limitation and strength of each approach according to the pollutant (CO_2 versus NOx). The paper is organised into four sections. First, it offers a review of the literature on RDE (Section 1) followed by the used material and methods (Section 2). Results from field measurements and calibration and validation of emission models are presented and discussed in Section 3 while last section shows the conclusions of the study (Section 4).

2. Material and Methods

2.1. Monitoring Campaigns

Experimental campaigns were performed in one diesel (V1) and one petrol (V2) passenger cars (Segment B and Euro 6-c). The vehicles are representative of the European vehicle fleet (Ciferri, 2020) and have the following characteristics: i) model year: 2019; ii) mileage: 5 600 km (V1) and 2 500 km (V2); iii) transmission type: 6-speed manual (V1) and 5-speed manual (V2); iv) engine displacement: 1 248 cm^3 (V1) and 999 cm^3 (V2); v) number of cylinders: 4 (V1) and 3 (V2); vi) combined CO_2 WLTP: 119 g.km^{-1} (V1) and 118 g.km^{-1} (V2). Tests were carried out

in Aveiro region (Portugal) in one origin-destination pair with three alternative routes (R1, R2 and R3), as depicted in Fig. 1. The studied location was selected due to its variability in terms of speed limits, traffic flow, traffic control treatments, slopes, and road types (urban, extra-urban and highways), which are representative of real driving conditions (Fernandes et al., 2019, 2021). Most of the rural roads, in blue colour, are at the beginning and/or ending of each route where the vehicles were driven between 50 and 90 km.h^{-1}. Traffic conditions and traffic controls did not allow to perform all this section at the planned speed. The highway road sections, in red colour, were driven with a speed higher than 90 km.h^{-1}. Concerning the urban section, which is remarked in yellow, it includes three signalized intersections, one compact two-lane roundabouts, and one stop-controlled intersection.

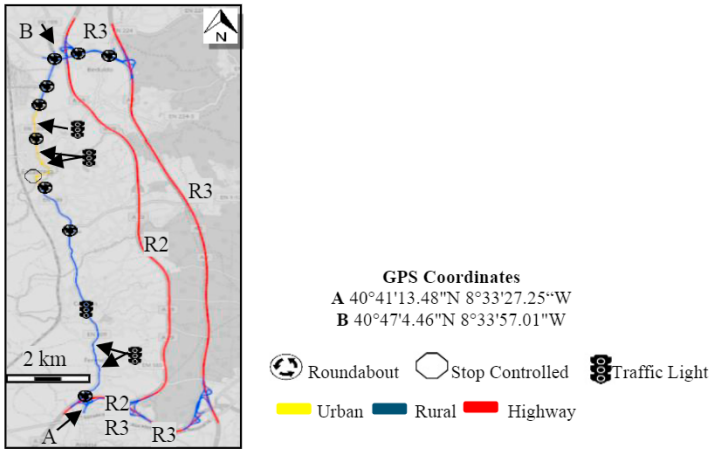

Fig. 1. Specific route of RDE tests in Aveiro region. Background Map Source [Open Street Maps].

The 3DATX ParSYNC integrated PEMS (3DATX, 2018) was used to measure exhaust emissions at a frequency of 1 Hz. The system comprises two gas analyses that measure volume fractions of CO_2 with non-dispersive infrared sensors, and nitric oxide (NO) and nitrogen dioxides (NO_2) with electrochemical cells. A Bluetooth OBD-II device was connected to the car's ECU device to collect main car engine data, such as OBD speed, mass air flow (MAF), MAP, RPM, engine load, air-to-fuel ratio (AFR), and intake air temperature (IAT). All measurements were carried out during working days for both morning and afternoon periods to obtain a wide range of traffic characteristics. Ambient temperatures ranged from 13 to 15ºC during the tests. The method described by Regulatory Information 40 CFR 86.144 was used to compute mass per-time exhaust emissions from PEMS output data using MAF and AFR reported via the OBD. Fernandes et al. (2021) provides full details pertaining to the calculations of mass per time-based tailpipe emission rates, data processing, quality assurance and trips verification.

2.2. Predictive Emission Models

For speed-based models, parabolic-shaped curves were used to correlate speed and emissions (Yao & Song, 2013) using least squares fitting technique to find the best-fitting curve for each speed interval with take into account route type characteristics: s1 ≤ 50 km.h^{-1}; 50 < s2 ≤ 90 km.h^{-1}; s3 > 90 km.h^{-1}.

The development of IOVs models was made by testing the most significant parameters on CO_2 and NOx emission rates. Prior studies have been showing that the variability in emission rates can be better explained by the product of MAP and RPM ($P_{\mathrm{MAP\times RPM}}$) than MAP and RPM separately (Hu et al., 2016). Having this in mind, a model in the form of Equation 1 was used (Fernandes et al., 2019):

$$m_{IOV,j,\mathrm{w,pred}} = c\frac{C_{\log}}{a'}\left(P_{\mathrm{MAP\times RPM}}\right)^{n} - \frac{b'}{a'} \tag{1}$$

where $m_{IOV,j,\mathrm{w,pred}}$ is the predicted mass flow rate of pollutant j, $j \in J$, $J = \{CO_2, \mathrm{NOx}\}$ and car w, $w \in W$, $W = \{\mathrm{V1,V2}\}$ (g.s^{-1}), c is the fitted scaling parameter, $C_{\log}$ represents a log-transformation bias correction factor, n is the power

parameter, a' represents the fitted slope, and b' is the model intercept.

Since engine air flow can be also influenced by reported IAT (Hu et al., 2016), a regression analysis between emission rates and this parameter was also conducted.

VSP-modal approach centred on binning emission rates in fourteen modes that reflects deceleration, idling, cruise, and acceleration driving situations. Each second-by-second estimate of VSP was stratified into 14 bins and then the average CO_2 and NOx emission rates for each bin were computed. Equation 2 applies VSP using parameter values to specific case of a typical passenger car (USEPA, 2002):

$$VSP_i = v_i\left[1.1a_i + 9.81r + 0.132\right] + 0.000302.v_i^3 \quad (2)$$

where VSP_i is the Vehicle Specific Power in the second of travel i (kW.ton^{-1}), v_i the instantaneous OBD speed in the second of travel i (m.s^{-1}), a_i is the acceleration in the second of travel i (m.s^{-2}), and r is the road grade (slope).

Driving volatility was characterized by means of vehicle acceleration and vehicular jerk, in which 9 combinations of vehicular jerk types were used to represent all driving behaviours. Jerk types 1 to 3 represent acceleration episodes, jerk types 4-6 deceleration episodes, jerk types 7-8 alternate acceleration and deceleration, and jerk type 9 is associated to cruise speed (Zhang et al., 2020). These types were computed for two consecutive seconds, as suggested by (Zhang et al., 2020; Fernandes et al., 2021). For each jerk type, correlations between engine load parameters and CO_2 and NOx emission rates were established using power-shape curves.

3. Results

For each of the 2 passenger cars, more than 12 000 s (road coverage of 125 km) of valid PEMS and OBD data were collected. The validation of the trips was confirmed that all trips fulfilled the RDE criteria concerning the ninety-five percentile of the product of vehicle speed and positive accelerations higher than 0.1 m.s^{-2}, and relative positive acceleration (EC, 2017). From these results, values of average mass trip emissions were computed. The differences between average field and vehicle-type approval CO_2 were 18% and 4% for V1 and V2, respectively. With respect to NOx, the average trip-value for V1 was 3.27 g.km^{-1}, which is below the NOx emission limit of 3.65 g.km^{-1} (White et al., 2018), while the average trip-value for V2 was 0.05 g.km^{-1}.

Multiple pairwise tests between route types were performed to evaluate the effect of speed intervals, VSP modes and jerk types on emission rates. The null hypothesis of the test is that the emission means values among speed intervals (s_1,s_2,s_3), VSP modes (1-14) and jerk types (1-9) are equal at a significance level of 5%. All p-values for speeds intervals were less than .05, which implied that this variable appeared to be a major explanatory variable of the CO_2. Approximately 75% and 50% of pair combinations of VSP modes and jerk types, respectively, showed to be statistically significant for CO_2 at level of 5%. The results for jerk types showed 22% and 33% of pair combinations exhibiting statistically significance for NOx, which may be possibly due to low frequency of specific jerk types.

After that, CO_2 and NOx predictive models were developed based on 70% of each car training data set (Liu et al., 2017). The fitted equations for CO_2 and NOx emission rates by speed interval are given by Eq. 3 to 6. The R^2 values were generally higher for speed values above 90 km.h^{-1}. For V2, the NOx speed-based models had R^2 values of less than 0.24, thus indicating poor fit. One reason behind this result was measured NOx emission rates that were below the detection limit of PEMS for nearly 60% of the second-by-second emission rates for this car.

$$m_{speed,CO2_{V1}} = \begin{cases} 0.000316s^2 + 0.002906s + 0.324582 \ \left(R^2 = 0.33, Fsig < 0.01\right), \ s \le 50\text{km/h} \\ -0.00187s^2 + 0.311689s - 9.70259 \ \left(R^2 = 0.39, Fsig < 0.01\right), \ 50 < s \le 90\text{km/h} \\ 0.00057s^2 + 0.000972s - 3.22016 \ \left(R^2 = 0.62, Fsig < 0.01\right), \ \text{otherwise} \end{cases} \quad (3)$$

$$m_{speed,CO2_{V2}} = \begin{cases} 0.000179s^2 + 0.029543s + 0.486966 \ \left(R^2 = 0.46, Fsig < 0.01\right), \ s \le 50\text{km/h} \\ -0.00142s^2 + 0.268755s - 7.73993 \ \left(R^2 = 0.37, Fsig < 0.01\right), \ 50 < s \le 90\text{km/h} \\ 0.001216s^2 - 0.24165s + 17.25748 \ \left(R^2 = 0.49, Fsig < 0.01\right), \ \text{otherwise} \end{cases} \quad (4)$$

$$m_{speed,NOx_{V1}} = \begin{cases} 0.006389s^2 + 0.0025112s + 2.523203 \ \left(R^2 = 0.36, Fsig < 0.01\right), \ s \le 50\text{km/h} \\ -0.09108s^2 + 13.67333s - 447.009 \ \left(R^2 = 0.36, Fsig < 0.01\right), \ 50 < s \le 90\text{km/h} \\ 0.212289s^2 - 42.0798s + 2116.014 \ \left(R^2 = 0.53, Fsig < 0.01\right), \ \text{otherwise} \end{cases} \quad (5)$$

$$m_{speed,NOx_{V2}} = \begin{cases} -0.00074s^2 + 0.065617s + 0.570557 \ \left(R^2 = 0.23, Fsig < 0.01\right), \ s \le 50\text{km/h} \\ 0.006321s^2 - 0.72271s + 22.83853 \ \left(R^2 = 0.20, Fsig < 0.01\right), \ 50 < s \le 90\text{km/h} \\ 0.008948s^2 - 2.41252s + 167.7857 \ \left(R^2 = 0.21, Fsig < 0.01\right), \ \text{otherwise} \end{cases} \quad (6)$$

where $m_{speed,CO2,V1}$ and $m_{speed,CO2V2}$ are the estimated CO_2 based on speed for V1 and V2, respectively (g.s^{-1}), and $m_{speed,NOx,V1}$ and $m_{speed,NOxV2}$ are the estimated NOx based on speed for V1 and V2, respectively (mg.s^{-1}).

Fig. 2 a-b depicts the relationships between CO_2 emissions rates and $P_{MAP\times RPM}$; the adjusted R^2 values for V1 and V2 were 0.57 and 0.92, respectively. A comparison of NOx emission rates predicted by the $P_{MAP\times RPM}$ versus measured NOx emission rates revealed that the variability in NOx emission rates was better explained in the diesel passenger car (Fig. 2 c-d). The resulting R^2 was 0.65, which is better than the R^2 of 0.37 of V2 NOx model. A portion of V1 data had considerably high NOx emission rates compared with the fitted model, ranging up to 800 mg.s^{-1}. This happens because engine goes into open-loop operation where Electronic Car Unit (ECU) computes AFR based on inputs from the coolant and MAF sensors. Since these events represent a different operating condition than obtained in most of the data set, V1-NOx data less than 0.3 g.s^{-1} (< 0.4% of travel time) were stratified. The relationship between IAT and emissions rates did not result in any correlation for both passenger cars. Accordingly, the prediction of exhaust emission rates using IOVs was done based on $P_{MAP\times RPM}$ alone. After bias correction (Eq. 1), the predicted equations by pollutant and car are given in Eq.7 to 10.

$$m_{IOV,CO2_{V1}} = 2.98\times10^{-3}\times\left(P_{MAP\times RPM}\right)^{1.79} - 0.19 \ \left(R^2 = 0.57, Fsig < 0.01\right) \quad (7)$$

$$m_{IOV,CO2_{V2}} = 1.05\times\left(P_{MAP\times RPM}\right)^{1.05} - 0.33 \ \left(R^2 = 0.92, Fsig < 0.01\right) \quad (8)$$

$$m_{IOV,NOx_{V1}} = 5.39\times10^{-2}\times\left(P_{MAP\times RPM}\right)^{1.91} - 4.37 \ \left(R^2 = 0.65, Fsig < 0.01\right) \quad (9)$$

$$m_{IOV,NOx_{V2}} = 1.29\times\left(P_{MAP\times RPM}\right)^{0.82} \ \left(R^2 = 0.37, Fsig < 0.01\right) \quad (10)$$

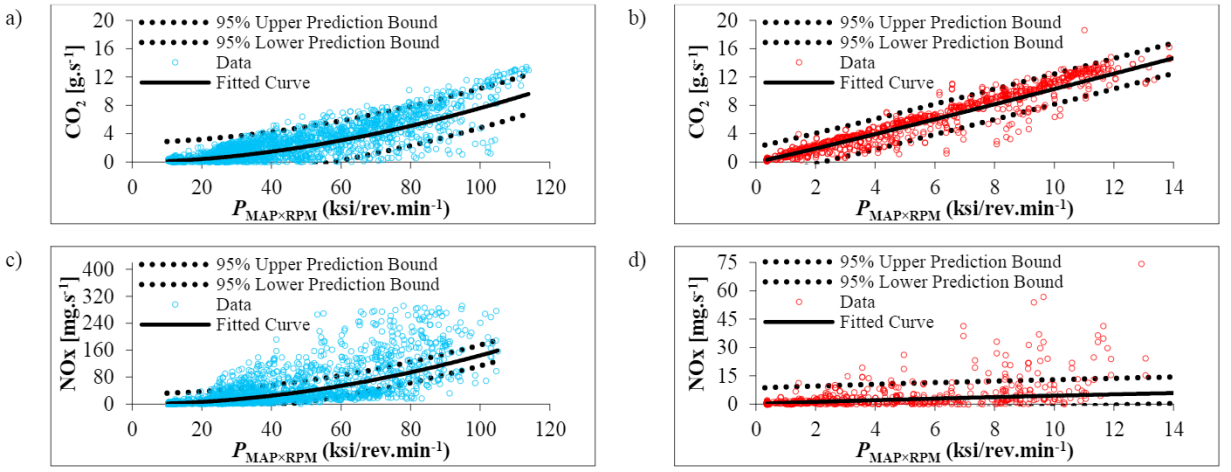

Fig. 2. Emission rates versus IOVs: (a) V1 – CO_2; (b) V2 – CO_2; (c) V1 – NOx; (d) V2 – NOx.

The VSP modal emission rates for the V1 and V2 are depicted in Fig. 3 a-d. The data set of V1 and V2 results revealed that CO_2 and NOx emission rates generally increased for positive VSP values (from modes 3 to 14), which is consistent with prior works in other ICE powertrains (Coelho et al., 2009; Fernandes et al., 2019). The values of coefficient of variability for CO_2 were higher (0.13-2.17, depending on the VSP mode and vehicle) than those obtained for NOx (0.96-13.46, depending on the VSP mode and vehicle). The coefficient interval on the NOx mean was relatively wide at VSP modes higher than 8 because the small sample size of less than 150 s.

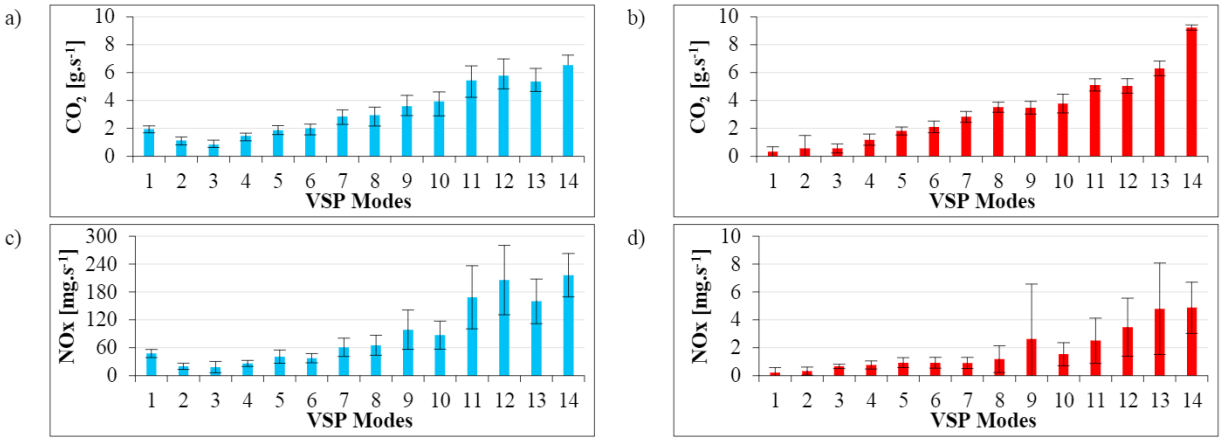

Fig. 3. VSP modal emission rates (with 95% confidence intervals): (a) V1 – CO_2; (b) V2 – CO_2; (c) V1 – NOx; (d) V2 – NOx.

The relationship between emission rates and jerk types was performed using power functions of the $P_{MAP \times RPM}$. The predicted models for cruise and volatile types had a similar form to those obtained in the Eq.7 to 10 but stratified into vehicular jerk classification types. Table 1 lists all R^2 for the fitted jerk-based models versus measured rates for CO_2 and NOx. Since the fitted models of both jerk types 4 and 5 were similar, one equation was used to represent these volatile states (Zhang et al., 2020). For all nine jerk types, the values of R^2 were greater than or equal to 0.45, 0.74, 0.50 and 0.25 for V1-CO_2, V2-CO_2, V1-NOx, and V2-NOx, respectively. The p-value for both the fitted scaling and power parameters were lower than 0.01, thus indicating statistical significance.

Table 1. Jerk-based models and resulting coefficients of determination for emission rates for both vehicles

Car	Specie	Jerk Type	Expression	Fitted Model	R^2	*Fsig*
V1	CO_2	1	$a_i = a_{i+1} \rightarrow j = 0$ m.s^{-3}	$5.38 \times 10^{-3} \times (P_{MAP \times RPM})^{1.69} - 0.05$	0.54	< 0.05
		2	$a_i > a_{i+1} \rightarrow j < 0$ m.s^{-3}	$2.89 \times 10^{-3} \times (P_{MAP \times RPM})^{1.82} - 0.20$	0.49	< 0.05
		3	$a_i < a_{i+1} \rightarrow j > 0$ m.s^{-3}	$2.13 \times 10^{-3} \times (P_{MAP \times RPM})^{1.87} - 0.13$	0.51	< 0.05
		4,5	$a_i = a_{i+1} \rightarrow j = 0$ m.s^{-3} (4) $a_i < a_{i+1} \rightarrow j > 0$ m.s^{-3} (5)	$1.66 \times 10^{-3} \times (P_{MAP \times RPM})^{1.97} - 0.04$	0.59	< 0.05
		6	$a_i < a_{i+1} \rightarrow j > 0$ m.s^{-3}	$7.99 \times 10^{-4} \times (P_{MAP \times RPM})^{2.16} - 0.08$	0.61	< 0.05
		7	$a_i > a_{i+1} \rightarrow j < 0$ m.s^{-3}	$6.02 \times 10^{-3} \times (P_{MAP \times RPM})^{1.62} - 0.42$	0.49	< 0.05
		8	$a_i < a_{i+1} \rightarrow j > 0$ m.s^{-3}	$2.09 \times 10^{-3} \times (P_{MAP \times RPM})^{1.89} - 0.14$	0.45	< 0.05
		9	$a_{i+1} = 0$ $(a_i = 0) \rightarrow j = 0$ m.s^{-3}	$3.61 \times 10^{-3} \times (P_{MAP \times RPM})^{1.74} - 0.17$	0.55	< 0.05
	NOx	1	$a_i = a_{i+1} \rightarrow j = 0$ m.s^{-3}	$2.77 \times 10^{-2} \times (P_{MAP \times RPM})^{2.18} - 8.43$	0.68	< 0.05
		2	$a_i > a_{i+1} \rightarrow j < 0$ m.s^{-3}	$3.42 \times 10^{-3} \times (P_{MAP \times RPM})^{2.61} - 2.01$	0.71	< 0.05
		3	$a_i < a_{i+1} \rightarrow j > 0$ m.s^{-3}	$9.94 \times 10^{-3} \times (P_{MAP \times RPM})^{2.37} - 2.34$	0.68	< 0.05
		4,5	$a_i = a_{i+1} \rightarrow j = 0$ m.s^{-3} (4) $a_i < a_{i+1} \rightarrow j > 0$ m.s^{-3} (5)	$5.01 \times 10^{-2} \times (P_{MAP \times RPM})^{2.09} - 6.01$	0.69	< 0.05
		6	$a_i < a_{i+1} \rightarrow j > 0$ m.s^{-3}	$2.87 \times 10^{-2} \times (P_{MAP \times RPM})^{2.22} - 4.61$	0.72	< 0.05
		7	$a_i > a_{i+1} \rightarrow j < 0$ m.s^{-3}	$2.86 \times 10^{-2} \times (P_{MAP \times RPM})^{2.10} - 7.22$	0.50	< 0.05
		8	$a_i < a_{i+1} \rightarrow j > 0$ m.s^{-3}	$2.90 \times 10^{-2} \times (P_{MAP \times RPM})^{2.09} - 4.95$	0.68	< 0.05
		9	$a_{i+1} = 0$ $(a_i = 0) \rightarrow j = 0$ m.s^{-3}	$2.00 \times 10^{-2} \times (P_{MAP \times RPM})^{2.26} - 3.13$	0.72	< 0.05
V2	CO_2	1	$a_i = a_{i+1} \rightarrow j = 0$ m.s^{-3}	$1.07 \times (P_{MAP \times RPM})^{1.05} - 0.58$	0.90	< 0.05
		2	$a_i > a_{i+1} \rightarrow j < 0$ m.s^{-3}	$1.09 \times (P_{MAP \times RPM})^{1.01} - 0.22$	0.90	< 0.05
		3	$a_i < a_{i+1} \rightarrow j > 0$ m.s^{-3}	$0.99 \times (P_{MAP \times RPM})^{1.07} - 0.31$	0.82	< 0.05
		4,5	$a_i = a_{i+1} \rightarrow j = 0$ m.s^{-3} (4) $a_i < a_{i+1} \rightarrow j > 0$ m.s^{-3} (5)	$0.89 \times (P_{MAP \times RPM})^{1.17}$	0.95	< 0.05
		6	$a_i < a_{i+1} \rightarrow j > 0$ m.s^{-3}	$1.06 \times (P_{MAP \times RPM})^{1.08} - 0.35$	0.91	< 0.05
		7	$a_i > a_{i+1} \rightarrow j < 0$ m.s^{-3}	$1.00 \times (P_{MAP \times RPM})^{1.02} - 0.24$	0.94	< 0.05
		8	$a_i < a_{i+1} \rightarrow j > 0$ m.s^{-3}	$1.20 \times (P_{MAP \times RPM})^{1.02} - 0.90$	0.74	< 0.05
		9	$a_{i+1} = 0$ $(a_i = 0) \rightarrow j = 0$ m.s^{-3}	$1.10 \times (P_{MAP \times RPM})^{1.02} - 0.33$	0.91	< 0.05
	NOx	1	$a_i = a_{i+1} \rightarrow j = 0$ m.s^{-3}	$2.06 \times (P_{MAP \times RPM})^{0.82} - 1.28$	0.28	< 0.05
		2	$a_i > a_{i+1} \rightarrow j < 0$ m.s^{-3}	$1.55 \times (P_{MAP \times RPM})^{0.88} - 0.91$	0.26	< 0.05
		3	$a_i < a_{i+1} \rightarrow j > 0$ m.s^{-3}	$2.44 \times (P_{MAP \times RPM})^{0.75} - 0.33$	0.25	< 0.05
		4,5	$a_i = a_{i+1} \rightarrow j = 0$ m.s^{-3} (4) $a_i < a_{i+1} \rightarrow j > 0$ m.s^{-3} (5)	$1.80 \times (P_{MAP \times RPM})^{0.80} - 0.76$	0.38	< 0.05
		6	$a_i < a_{i+1} \rightarrow j > 0$ m.s^{-3}	$1.79 \times (P_{RPM \times MAP})^{0.79} - 0.79$	0.36	< 0.05
		7	$a_i > a_{i+1} \rightarrow j < 0$ m.s^{-3}	$0.84 \times (P_{MAP \times RPM})^{1.09} - 0.13$	0.44	< 0.05
		8	$a_i < a_{i+1} \rightarrow j > 0$ m.s^{-3}	$0.14 \times (P_{MAP \times RPM})^{2.11}$	0.42	< 0.05
		9	$a_{i+1} = 0$ $(a_i = 0) \rightarrow j = 0$ m.s^{-3}	$2.44 \times (P_{MAP \times RPM})^{0.71} - 1.19$	0.35	< 0.05

Fig. 4 a-b illustrates the relative difference between emissions estimates from the testing dataset, using the proposed approaches in relation to the measured values. The results showed IOVs- and jerk-based models' capability to estimate CO_2 was reasonably accurate in comparison to R1 values; the differences were lower than 4% in both vehicles. VSP method achieved the highest differences in CO_2 emission rates for all analysed trips. Speed-based models generally resulted in overestimation of measured CO_2, but they had good predictions for V1 at R3 with only 6%. Conversely, in predicting NOx emissions, the models that used VSP as explanatory variables performed better than the models that used engine and/or vehicular jerk variables. This is due to VSP differentiated between closed-loop and open-loop control of the AFR. The jerk-based approach resulted in a higher overestimation of NOx (66% and 91% on average in V1 and V2, respectively) than the IOVs-based approach (39% and 70% on average in V1 and V2, respectively).

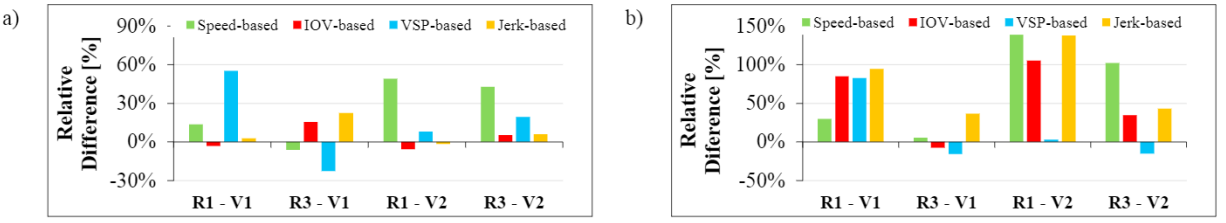

Fig. 4. Comparison of proposed approaches (in relation to the measured values): (a) CO_2; (b) NOx.

4. Conclusions

Empirical-based methods that used second-by-second tailpipe emissions, engine and driving volatility data for ICE to predict emissions rates were suggested. On-road emissions and engine activity data were collected from one petrol and diesel under RDE driving conditions. Four different approaches were then examined: i) speed-based intervals; ii) IOVs-based; iii) VSP-based; iv) driving volatility based on vehicular jerk behaviours. It was concluded that speed was a good explanatory variable in estimating CO_2 at driving speeds higher than 90 $km.h^{-1}$. IOVs based predictors of engine load ($P_{MAP \times RPM}$) were able to explain better the variability in CO_2 than NOx. The use of driving volatility as means of nine vehicular jerk types to represent cruise and volatile states agreed relatively well CO_2 data. Validation results confirmed that IOVs and jerk-based models achieved similar measured CO_2. However, they were worse in predicting NOx than a VSP-modal approach since the latter approach characterised closed-loop and open-loop control of the AFR. This research can contribute to the vehicle emission monitoring topic in three main aspects. First, it defines different driving behaviours regarding vehicular jerk and acceleration, which are well-demonstrated measures of unsafe driving decisions. Second, each of proposed approaches has advantages that relies in being less data intensive. Third, the developed models can be integrated directly into ECU to provide real-time emission rates. Although recent vehicles are equipped with eco-efficient driving modes to minimise fuel consumption, information about NOx is neglected. Models based on engine parameters neither include open-loop control of the air-to-fuel ratio, nor included the most relevant parameters of system catalyst reduction in diesel engines. A drawback of the study is the neglected effect of gear ratio choice on the emission rates at different constant speed values with different RPM in the development of IOVs models. There is the potential to enhance NOx model performance by examining other parameters such as catalytic temperature, variations in the nitrogen dioxides and NOx ratio and ammonia to NOx ratio. Next steps are devoted to the development of a graphical interface capable of remotely connect with ECU system to incorporate the proposed framework on a more practical way.

Acknowledgements

This work was supported by the projects UIDB/00481/2020 and UIDP/00481/2020 - FCT - Fundação para a Ciência e a Tecnologia; and CENTRO-01-0145-FEDER-022083 - Centro Portugal Regional Operational Programme (Centro2020), under the PORTUGAL 2020 Partnership Agreement, through the European Regional Development Fund; DICA-VE (POCI-01-0145-FEDER-029463) project funded by FEDER through COMPETE2020, and by national funds (OE), through FCT/MCTES; and "PAC Portugal AutoCluster for the Future" project, funded by P2020. E. Ferreira acknowledges the support the support for the FCT Ph.D. Scholarship UI/BD/151254/2021.

References

3DATX, 2018. 3-dimensional data analysis (3DATX) Corporation, Available from: http://www.3datx.com/, January 29, 2021.

ACEA, 2020. New passenger car registrations in the EU by alternative fuel type, European Automobile Manufacturers' Association, Available from: https://www.acea.be/uploads/press_releases_files/20190206_PRPC_fuel_Q4_2019_FINAL.pdf, January 15, 2021.

Chossière, G.P., Malina, R., Allroggen, F., Eastham, S.D., Speth, R.L., Barrett, S.R.H., 2018. Country- and manufacturer-level attribution of air quality impacts due to excess NOx emissions from diesel passenger vehicles in Europe. Atmospheric Environ. 189, 89-97.

Ciferri, L., 2020. Reign at Risk. Crain Communications Inc, Automotive News Europe, 30-31.

Coelho, M.C., Frey, H.C., Rouphail, N.M., Zhai, H., Pelkmans, L., 2009. Assessing methods for comparing emissions from gasoline and diesel light-duty vehicles based on microscale measurements. Transp Res D Transp. Environ. 14.2, 91-99.

Davison, J., Bernard, Y., Borken-Kleefeld, J., Farren, N.J., Hausberger, S., Sjödin, Å., Tate, J.E., Vaughan, A.R., Carslaw, D.C., 2020. Distance-based emission factors from vehicle emission remote sensing measurements. Sci. Total Environ. 739, 139688.

EC, 2017. European Comission, Available from: https://eur-lex.europa.eu/LexUriServ/LexUriServ.do?uri=OJ:L:2008:199:0001:0136:EN:PDF, January 29, 2021.

EEA, 2020a. Air quality in Europe — 2020 report. European Environment Agency, Available from: https://www.eea.europa.eu/publications/air-quality-in-europe-2020-report, January 14, 2021.

EEA, 2020b. Average CO_2 emissions from new cars and new vans increased again in 2019, European Environment Agency, Available from: https://www.eea.europa.eu/highlights/average-co2-emissions-from-new-cars-vans-2019. January 15, 2021.

Emisia, 2020. COPERT — COmputer Programme to calculate Emissions from Road Transport. Available from: https://www.emisia.com/, January 31, 2021.

EPA, 2020. MOVES and Related Models, Environmental Protection Agency, Available from: https://www.epa.gov/moves, January 14, 2021.

Faria, M., Baptista, P., Farias, T., 2017. Identifying driving behavior patterns and their impacts on fuel use, Transportation Research Procedia 27, 953-960.

Fernandes, P., Macedo, E., Bahmankhah, B., Tomás, R., Bandeira, J.M.,Coelho, M.C., 2019. Are internally observable vehicle data good predictors of vehicle emissions? Transp Res D Transp. Environt. 77, 252-270.

Fernandes, P., Tomás, R., Ferreira, E., Bahmankhah, B., Coelho, M.C., 2021. Driving aggressiveness in hybrid electric vehicles: Assessing the impact of driving volatility on emission rates. Applied Energy 284, 116250.

García-Contreras, R., Soriano, J.A., Fernández-Yáñez, P., Sánchez-Rodríguez, L., Mata, C., Gómez, A., Armas, O., Cárdenas, M.D., 2021. Impact of regulated pollutant emissions of Euro 6d-Temp light-duty diesel vehicles under real driving conditions. J. Clean. Prod. 286, 124927.

Gastaldi, M., Meneguzzer, C., Giancristofaro, R.A., Gecchele, G., Luccia, L.D., Prati, M.V., 2017. On-road measurement of CO2 vehicle emissions under alternative forms of intersection control, Transportation Research Procedia 27, 476-483.

Hu, J., Frey, H.C., Washburn, S.S., 2016. Comparison of Vehicle-Specific Fuel Use and Emissions Models Based on Externally and Internally Observable Activity Data. Transportation Research Record 2570.1, 30-38.

Kurtyka, K., Pielecha, K., 2019. The evaluation of exhaust emission in RDE tests including dynamic driving conditions, Transportation Research Procedia 40, 338-345.

Lijewski, P., Kozak, M., Fuć, P., Rymaniak, Ł., Ziółkowski, A., 2020. Exhaust emissions generated under actual operating conditions from a hybrid vehicle and an electric one fitted with a range extender. Transp Res D Transp. Environ. 78, 102183.

Liu, H., Gegov, A., Cocea, M., 2017. Unified Framework for Control of Machine Learning Tasks Towards Effective and Efficient Processing of Big Data. In W. Pedrycz, S.-M. Chen (Eds.), Data Science and Big Data: An Environment of Computational Intelligence (pp. 123-140).

Macedo, E., Tomás, R., Fernandes, P., Coelho, M.C., Bandeira, J.M., 2020. Quantifying road traffic emissions embedded in a multi-objective traffic assignment model. Transportation Research Procedia 47, 648-655.

Mannucci, P.M., Harari, S., Martinelli, I., Franchini, M., 2015. Effects on health of air pollution: a narrative review. Int Emerg. Med. 10-6, 657-662.

Söderena, P., Laurikko, J., Weber, C., Tilli, A., Kuikka, K., Kousa, A., Väkevä, O., Venho, A., Haaparanta, S., Nuottimäki, J., 2020. Monitoring Euro 6 diesel passenger cars NOx emissions for one year in various ambient conditions with PEMS and NOx sensors. Sci. Total Environ. 746, 140971.

Triantafyllopoulos, G., Dimaratos, A., Ntziachristos, L., Bernard, Y., Dornoff, J., Samaras, Z., 2019. A study on the CO_2 and NOx emissions performance of Euro 6 diesel vehicles under various chassis dynamometer and on-road conditions including latest regulatory provisions. Sci. Total Environ. 666, 337-346.

USEPA, 2002. Methodology for developing modal emission rates for EPA's multi-scale motor vehicle & equipment emission system. Report EPA420-R-02-027, United States Environmental Protection Agency.

White, L., Miles, A., Boocock, C., Cooper, J-G., Mills, S., 2018. A comparison of real driving emissions from Euro 6 diesel passenger cars with zero emission vehicles and their impact on urban air quality compliance, Report no. 8/1, Available from https://www.acea.be/uploads/statistic_documents/Economic_and_Market_Report_full-year_2018.pdf, January 25, 2021.

Yao, E., Song, Y., 2013. Study on Eco-Route Planning Algorithm and Environmental Impact Assessment. J Intell Transp. Syst. 17.1, 42-53.

Yazdani, B., Frey, H.C., 2014. Road grade quantification based on global positioning system data obtained from real-world vehicle fuel use and emissions measurements. Atmospheric Environ. 85, 179-186.

Zhang, L., Zhao, X., Khattak, A., 2020. A New Fuel Consumption Model Considering Vehicle's Speed, Acceleration and Jerk. Presented at the 99th Transportation Research Board Annual Meeting, 12-16 January, Washington D.C., U.S.